PCCP

ROYAL SOCIETY OF CHEMISTRY

PAPER

View Article Online
View Journal | View Issue

Cite this: *Phys. Chem. Chem. Phys.*, 2024, **26**, 16048

Benchmark *ab initio* characterization of the complex potential energy surfaces of the HOO^- + CH_3Y [Y = F, Cl, Br, I] reactions†

Domonkos A. Tasi * and Gábor Czakó *

The α-effect is a well-known phenomenon in organic chemistry, and is related to the enhanced reactivity of nucleophiles involving one or more lone-pair electrons adjacent to the nucleophilic center. The gas-phase bimolecular nucleophilic substitution (S_N2) reactions of α-nucleophile HOO^- with methyl halides have been thoroughly investigated experimentally and theoretically; however, these investigations have mainly focused on identifying and characterizing the α-effect of HOO^-. Here, we perform the first comprehensive high-level *ab initio* mapping for the HOO^- + CH_3Y [Y = F, Cl, Br and I] reactions utilizing the modern explicitly-correlated CCSD(T)-F12b method with the aug-cc-pV*n*Z [*n* = 2–4] basis sets. The present *ab initio* characterization considers five distinct product channels of S_N2: (CH_3OOH + Y^-), proton abstraction (CH_2Y^- + H_2O_2), peroxide ion substitution (CH_3OO^- + HY), S_N2-induced elimination (CH_2O + HY + HO^-) and S_N2-induced rearrangement ($CH_2(OH)O^-$ + HY). Moreover, besides the traditional back-side attack Walden inversion, the pathways of front-side attack, double inversion and halogen-bond complex formation have also been explored for S_N2. With regard to the Walden inversion of HOO^- + CH_3Cl, the previously unaddressed discrepancies concerning the geometry of the corresponding transition state are clarified. For the HOO^- + CH_3F reaction, the recently identified S_N2-induced elimination is found to be more exothermic than the S_N2 channel, submerged by ∼36 kcal mol^{-1}. The accuracy of our high-level *ab initio* calculations performed in the present study is validated by the fact that our new benchmark 0 K reaction enthalpies show excellent agreement with the experimental data in nearly all cases.

Received 11th March 2024,
Accepted 6th May 2024

DOI: 10.1039/d4cp01071j

rsc.li/pccp

I. Introduction

Theoretical and experimental investigations of the gas-phase bimolecular nucleophilic substitution (S_N2) reactions have gained increasing prominence since the 1970s.[1–10] In step with the progress of computational chemistry and experimental methodology,[11–16] the initially conceived simple picture of the elemental S_N2 reactions has been found to be incomplete, as it became apparent that along with the traditional Walden inversion and front-side attack, several alternative mechanisms may also occur depending on the reactants and the reaction conditions.[17–21]

Transcending the conventional reactions between halide ions and methyl halides, our understanding of S_N2 was also reshaped by the examination of reactions involving HO^-.[22–38] In 2002, Sun *et al.* investigated the HO^- + CH_3F S_N2 reaction by performing direct dynamics simulations and revealed that the reaction avoids the region of the deep H-bonded $CH_3OH\cdots F^-$ minimum in the exit channel.[22] Since then, other theoretical studies have uncovered a novel oxide ion substitution for the HO^- + CH_3F reaction utilizing quasi-classical trajectory (QCT), as well as, direct dynamics calculations.[39–41] Over the years, the primary focus has been on the dynamical characterization of the HO^- + CH_3I reaction.[42–48] Wester and co-workers examined several S_N2 reactions experimentally, including HO^- + CH_3I, with the crossed-beam ion-imaging technique.[10,14,49] Direct dynamics simulations were also performed by Hase and co-workers, paving the way for comprehensive experimental–theoretical studies of the HO^- + CH_3I reaction.[50–52] Furthermore, the present authors developed several global analytical *ab initio* potential energy surfaces (PESs) for HO^- + CH_3I at seven different levels of theory using the in-house Robosurfer program package.[53,54] Afterwards, on the final PES, which was confirmed to be the most suitable for further investigations, more than half a million trajectories were computed, comparing the results with the results of revised crossed-beam experiments

MTA-SZTE Lendület Computational Reaction Dynamics Research Group, Interdisciplinary Excellence Centre and Department of Physical Chemistry and Materials Science, Institute of Chemistry, University of Szeged, Rerrich Béla tér 1, Szeged H-6720, Hungary. E-mail: dtasi@chem.u-szeged.hu, gczako@chem.u-szeged.hu

† Electronic supplementary information (ESI) available: Benchmark Cartesian coordinates (Å) and energies (E_h) of the stationary points. See DOI: https://doi.org/10.1039/d4cp01071j

in order to analyze the dynamics of the reaction in a more detailed manner.[55] Recently, the mode specificity in the dynamics of the reaction was also studied at several collision energies by exciting certain vibrational modes of the reactants.[56,57]

Besides considering di- or polyatomic 'normal' nucleophiles (*e.g.*, HO^-, CN^-, NH_2^-, PH_2^- *etc.*),[10,24,58–63] a significant emphasis has been placed on α-nucleophiles (*e.g.*, HOO^-, ClO^-, BrO^-, CH_3OO^-, $HOHN^-$, NH_2O^-, *etc.*) participating in S_N2 reactions.[8,9,64–71] In the case of these α-nucleophiles, one or more lone-pair electrons are located on the atom adjacent to the nucleophilic center, inducing enhanced reactivity compared to that expected from the Brønsted-type correlation.[72] This phenomenon is known as the α-effect.[73] While the existence of the α-effect was beyond doubt in solution, the situation was not as clearly defined in the gas phase.[72,74,75] By comparing the branching ratios for the reactions of HO^- and HOO^- with methyl formate, DePuy and co-workers concluded that HOO^- does not show the α-effect in the gas phase.[76] In addition, Villiano *et al.* unveiled that a noticeable α-effect cannot be observed for the $HOO^-/ClO^-/BrO^-$ + CH_3R (R = CH_3, CH_3CH_2, *etc.*) systems, as well.[65] In contrast, the opposite of these findings has been confirmed, and several studies have verified that the α-effect stems from the intrinsic properties of α-nucleophiles validating the manifestation of this phenomenon in the gas phase.[77–85] However, the identification of these intrinsic properties of α-nucleophiles remained disputed.[86–93] Recently, Hamlin *et al.* reported an extensive theoretical survey on the origin of the α-effect in the gas phase.[71] They employed the activation strain model of reactivity in combination with Kohn–Sham molecular orbital theory and arrived at the conclusion that the adjacent atom of α-nucleophiles induces a reduction in Pauli repulsion between the reactants by polarizing orbital density away from the nucleophilic center. As a result, an enhancement of the reactivity can be obtained for α-nucleophiles compared to their 'normal' counterparts.

Regarding S_N2 reactions involving HOO^-, several theoretical investigations have concentrated on the stationary-point and dynamical characterization, as well.[74,88,94–97] In the course of the aforementioned α-effect examinations, the stationary points of the corresponding Walden-inversion pathways were determined for several S_N2 reactions of HOO^- at various levels of theory. The $HOO^-\cdots CH_3Y \rightarrow [HOO\cdots CH_3\cdots Y]^- \rightarrow CH_3OOH\cdots Y^-$ path was explored by Evanseck *et al.* for Y = Cl at the level of HF/6-31+G(d).[74] Later, in the theoretical surveys of Ren *et al.*, the geometries of the $[HOO\cdots CH_3\cdots Y]^-$ transition states were optimized in the case of Y = F and Cl at the MP2/6-31+G(d) level of theory, and the corresponding energies were determined with the G2(+) method.[78,79] Associated with the microsolvated variants of the HOO^- + CH_3Cl S_N2 reaction, the unsolvated Walden-inversion pathways were also characterized in the studies of Thomsen *et al.*[88] and Hu *et al.*[97] utilizing the MP2/6-311++G(d,p) level of theory in combination with G3 and CCSD(T)/aug-cc-pVTZ energy calculations, respectively. The most thorough *ab initio* mapping was achieved by Wu *et al.* in the case of the $HOO^-(H_2O)_n$ + CH_3Y [Y = F, Cl, Br, I; n = 0, 1, 2] S_N2 reactions, whereby they identified two H-bonded stationary points in the entrance channel, as well.[96] The dynamics of the $HOO^-(H_2O)_n$ + CH_3Cl reactions, where n = 0 or 1, was also examined with direct dynamics simulations.[94,95] It is noteworthy that, based on the earlier work of Anick *et al.*,[98] the only stable structure for the singly hydrated hydroperoxide ion is $HO^-(HOOH)$, which indicates that in the S_N2 reaction with CH_3Cl, two distinct pathways may be possible, leading to the CH_3OOH + Cl^- + H_2O and CH_3OH + Cl^- + H_2O_2 products. Recently, dynamics simulations performed by Zhao *et al.*[95] have substantiated that both reaction routes are viable, indicating the fact that a single solvent water molecule can induce a new nucleophile in S_N2 reactions, which opens the door for an alternative pathway. Moreover, for the unsolvated HOO^- + CH_3Cl reaction, similar to the case of ClO^- + CH_3Cl,[65,69] a novel non-S_N2 pathway generating the CH_2O + HCl + HO^- products was also unveiled. Besides the dynamical description, the PES of the considered product channels of the HOO^- + CH_3Cl reaction was mapped at the MP2/6-31+G(d,p) level of theory.[95]

In the present work, based on the prominent attention paid to the S_N2 reactions involving hydroperoxide ions, we perform a comprehensive benchmark *ab initio* characterization of HOO^- + CH_3Y [Y = F, Cl, Br and I] using the explicitly-correlated CCSD(T)-F12b method with the aug-cc-pV*n*Z [n = 2 (D), 3 (T) and 4 (Q)] basis sets. Besides the traditional Walden-inversion path, we analyze the halogen-bonded complex mechanism[48] and the possible S_N2 retention routes of front-side attack and double inversion.[19] We identify the stationary points of the proton-abstraction channel, as well; furthermore, relying on the previous study of Xie and co-workers,[95] our high-level stationary-point mapping also considers other possible pathways. Detailed insights into the applied *ab initio* methods can be found in Section II. In the subsequent Section III, a comprehensive description and discussion of the results are presented, followed by a brief summary of the work in Section IV.

II. Computational details

The stationary points of the title reactions are searched and preoptimized using the second-order Møller–Plesset perturbation theory (MP2)[99] with the augmented correlation-consistent polarized-valence-double-ζ (aug-cc-pVDZ) basis set.[100] The exploration of the stationary points was conducted based on previous studies and chemical intuition;[24,38,95] nevertheless, it is important to note that automated methods and approaches for identifying reaction pathways and stationary points in chemical reactions are becoming more and more prevalent.[101–103] Thereafter, in order to attain more accurate geometries, energies and harmonic frequencies for the stationary points, the explicitly-correlated coupled-cluster singles, doubles, and perturbative triples (CCSD(T)-F12b) method[104–106] is utilized with the aug-cc-pVDZ and aug-cc-pVTZ basis sets.[100] To achieve a more in-depth mapping, intrinsic reaction coordinate (IRC) computations are also carried out from the saddle points at the MP2/aug-cc-pVDZ level of theory. In order to avoid any spurious stationary point, it is

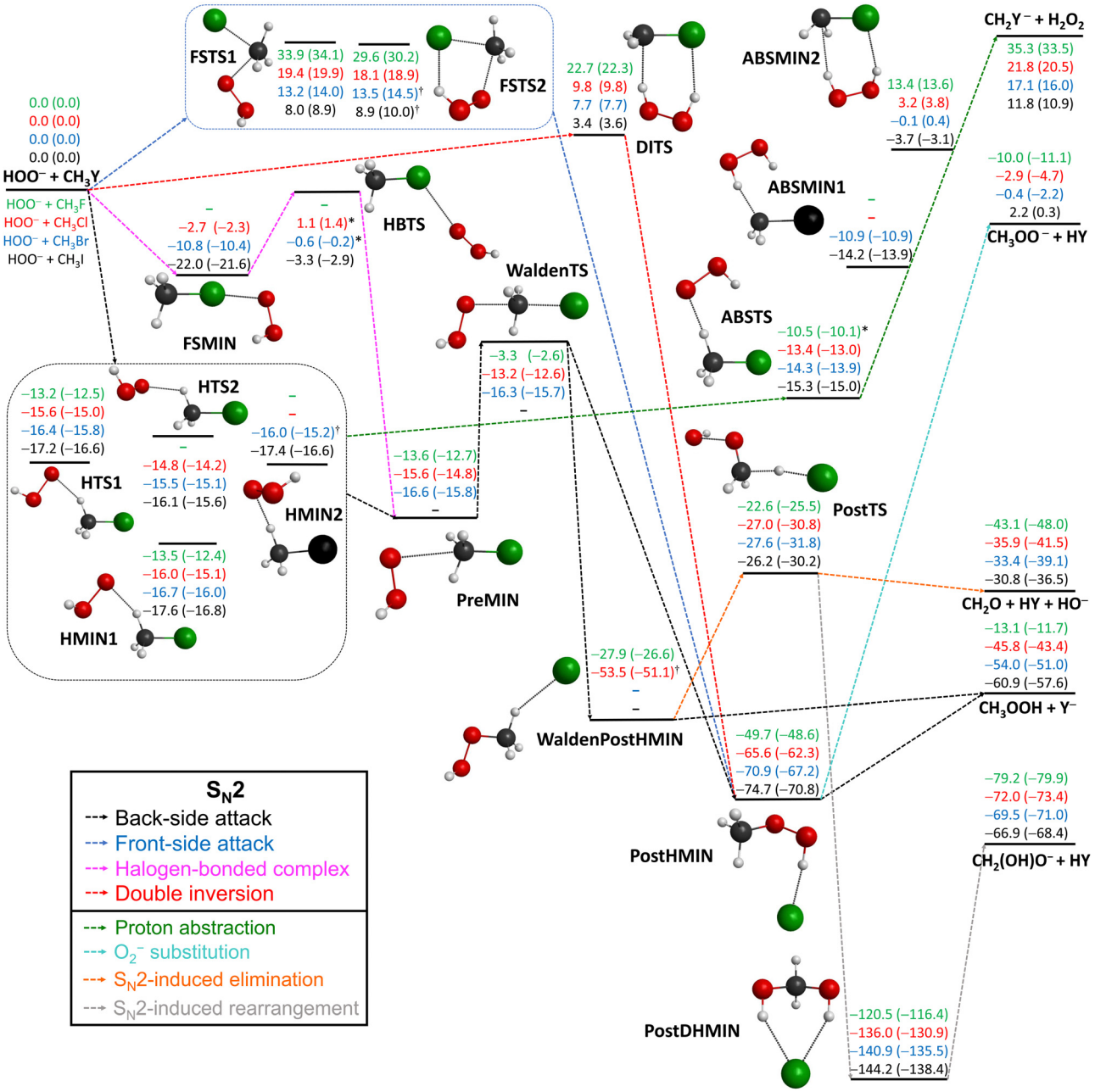

Fig. 1 Schematic representation of the complex potential energy surfaces of the HOO^- + CH_3Y [Y = F, Cl, Br, I] reactions presenting the classical (adiabatic) CCSD(T)-F12b/aug-cc-pVQZ (+ΔZPE[CCSD(T)-F12b/aug-cc-pVTZ]) relative energies (kcal mol^{-1}) of the stationary points along the possible reaction routes. †MP2/aug-cc-pVDZ structure; *CCSD(T)-F12b/aug-cc-pVDZ structure.

important to note that for all geometry optimizations, the default (3×10^{-4}) required accuracy of the optimized gradient is changed to 10^{-5} in atomic units. Small-core relativistic effective core potentials (ECPs)[107] are employed for Br and I, and the aug-cc-pV*n*Z-PP [*n* = 2–4] basis sets are applied to replace the inner-core $1s^2\ 2s^2\ 2p^6$ (Br) and $1s^2\ 2s^2\ 2p^6\ 3s^2\ 3p^6\ 3d^{10}$ (I) electrons. For the stationary points identified in the present work, the computed T_1-diagnostic values are below 0.02 in every case, except for FSTS and FSTS2 (see Fig. 1), where the values are between 0.02 and 0.04, validating that the multi-reference character is not a probable issue for the HOO^- + CH_3Y [Y = F, Cl, Br and I] systems. The benchmark classical (adiabatic) relative energies are computed for the CCSD(T)-F12b/aug-cc-pVTZ structures as follows:

$$\Delta E[\text{CCSD(T)-F12b/aug-cc-pVQZ}]\ (+\Delta\text{ZPE}[\text{CCSD(T)-F12b/aug-cc-pVTZ}]), \quad (1)$$

where ΔZPE is the harmonic zero-point energy correction. The *ab initio* calculations are performed with the Molpro program package.[108]

Table 1 Benchmark classical and adiabatic energies (kcal mol^{-1}) of the stationary points relative to the reactants for the possible pathways of the HOO^- + CH_3Y [Y = F, Cl, Br, I] reactions

	MP2	CCSD(T)-F12b				
HOO^- + CH_3F	DZ[a]	DZ[b]	TZ[c]	QZ[d]	ΔZPE[e]	Adiabatic[f]
HMIN1	−14.41	−13.95	−13.69	−13.47	1.09	−12.38
HTS1	−14.00	−13.49	−13.32	−13.15	0.67	−12.49
PreMIN	−14.45	−14.01	−13.80	−13.59	0.84	−12.74
WaldenTS	−6.77	−3.37	−3.44	−3.27	0.66	−2.61
FSTS1	29.87	33.40	33.50	33.87	0.25	34.12
FSTS2	25.76	29.26	29.28	29.64	0.59	30.23
DITS	21.68	21.81	22.37	22.72	−0.37	22.35
PostHMIN	−53.64	−50.43	−49.99	−49.74	1.11	−48.63
WaldenPostHMIN	−32.77	−28.62	−28.08	−27.91	1.26	−26.65
ABSTS	−11.38	−11.00	−10.71[g]	−10.52[g]	0.44[g]	−10.08[g]
ABSMIN2	12.34	12.43	13.00	13.37	0.28	13.65
PostTS	−28.42	−23.65	−22.93	−22.62	−2.89	−25.51
PostDHMIN	−127.02	−121.31	−120.63	−120.45	4.07	−116.38
HOO^- + CH_3Cl	MP2[a]	DZ[b]	TZ[c]	QZ[d]	ΔZPE[e]	Adiabatic[f]
HMIN1	−17.02	−16.26	−16.14	−15.97	0.89	−15.08
HTS1	−16.57	−15.78	−15.74	−15.62	0.62	−15.00
HTS2	−15.45	−15.04	−14.98	−14.82	0.59	−14.23
FSMIN	−1.81	−3.25	−2.87	−2.73	0.47	−2.27
HBTS	1.54	0.80	1.06[g]	1.14[g]	0.26[g]	1.40[g]
PreMIN	−16.35	−15.73	−15.72	−15.57	0.79	−14.78
WaldenTS	−14.39	−13.03	−13.33	−13.24	0.62	−12.62
FSTS1	18.84	19.20	19.19	19.40	0.48	19.88
FSTS2	18.12	17.44	17.80	18.07	0.85	18.93
DITS	9.64	9.13	9.61	9.82	−0.02	9.81
PostHMIN	−68.49	−65.91	−65.58	−65.61	3.26	−62.34
WaldenPostHMIN	−57.10	−53.75[h]	−53.44[h]	−53.55[h]	2.48[h]	−51.07[h]
ABSTS	−14.49	−13.79	−13.59	−13.43	0.45	−12.98
ABSMIN2	3.08	2.71	3.03	3.23	0.52	3.75
PostTS	−38.33	−27.93	−27.17	−27.01	−3.75	−30.76
PostDHMIN	−141.29	−136.29	−135.89	−136.00	5.14	−130.86
HOO^- + CH_3Br	MP2[a]	DZ[b]	TZ[c]	QZ[d]	ΔZPE[e]	Adiabatic[f]
HMIN1	−17.61	−17.21	−16.92	−16.74	0.74	−15.99
HMIN2	−17.22	−16.57[h]	−16.18[h]	−15.97[h]	0.82[h]	−15.15[h]
HTS1	−17.13	−16.72	−16.49	−16.35	0.54	−15.81
HTS2	−15.90	−15.92	−15.71	−15.53	0.42	−15.11
FSMIN	−10.48	−11.07	−10.89	−10.76	0.37	−10.39
HBTS	−0.36	−0.67	−0.70[g]	−0.62[g]	0.39[g]	−0.23[g]
PreMIN	−16.87	−16.88	−16.73	−16.57	0.79	−15.77
WaldenTS	−16.35	−16.41	−16.45	−16.32	0.62	−15.70
FSTS1	14.09	12.96	12.98	13.17	0.78	13.95
FSTS2	14.10	13.18[h]	13.29[h]	13.55[h]	0.95[h]	14.50[h]
DITS	7.23	6.88	7.42	7.69	0.05	7.73
PostHMIN	−72.09	−71.45	−70.85	−70.93	3.71	−67.22
ABSTS	−15.27	−14.80	−14.48	−14.30	0.41	−13.89
ABSMIN1	−11.03	−11.55	−11.18	−10.89	0.00	−10.90
ABSMIN2	0.38	−0.79	−0.37	−0.12	0.57	0.45
PostTS	−40.96	−28.82	−27.82	−27.63	−4.16	−31.80
PostDHMIN	−144.57	−141.54	−140.79	−140.94	5.48	−135.46
HOO^- + CH_3I	MP2[a]	DZ[b]	TZ[c]	QZ[d]	ΔZPE[e]	Adiabatic[f]
HMIN1	−18.52	−18.05	−17.75	−17.57	0.72	−16.84
HMIN2	−18.45	−17.96	−17.60	−17.40	0.79	−16.61
HTS1	−18.02	−17.56	−17.31	−17.17	0.53	−16.64
HTS2	−16.44	−16.51	−16.27	−16.10	0.54	−15.56
FSMIN	−22.36	−22.28	−22.11	−22.03	0.44	−21.59
HBTS	−2.65	−3.19	−3.37	−3.30	0.40	−2.90
FSTS1	9.16	7.85	7.91	8.04	0.87	8.91
FSTS2	10.01	8.46[h]	8.67[h]	8.93[h]	1.08[h]	10.01[h]
DITS	3.40	2.68	3.11	3.36	0.19	3.55

Table 1 (*continued*)

$HOO^- + CH_3I$	MP2[a]	DZ[b]	TZ[c]	QZ[d]	ΔZPE[e]	Adiabatic[f]
PostHMIN	−75.63	−75.15	−74.52	−74.74	3.94	−70.80
ABSTS	−16.32	−15.83	−15.48	−15.30	0.28	−15.02
ABSMIN1	−14.52	−14.76	−14.42	−14.15	0.28	−13.88
ABSMIN2	−2.98	−4.37	−3.97	−3.75	0.66	−3.09
PostTS	−36.02	−27.58	−26.36	−26.15	−4.08	−30.23
PostDHMIN	−147.56	−144.70	−143.92	−144.19	5.79	−138.40

[a] MP2/aug-cc-pVDZ. [b] CCSD(T)-F12b/aug-cc-pVDZ. [c] CCSD(T)-F12b/aug-cc-pVTZ. [d] CCSD(T)-F12b/aug-cc-pVQZ at CCSD(T)-F12b/aug-cc-pVTZ geometry. [e] ΔZPE(CCSD(T)-F12b/aug-cc-pVTZ). [f] QZ + ΔZPE. [g] CCSD(T)-F12b/aug-cc-pVDZ geometry and frequencies. [h] MP2/aug-cc-pVDZ geometry and frequencies.

III. Results and discussion

The complex PESs of the $HOO^- + CH_3Y$ [Y = F, Cl, Br and I] reactions showing the benchmark classical (adiabatic) relative energies of the stationary points along the considered pathways are presented in Fig. 1. The *ab initio* energies determined at the MP2/aug-cc-pVDZ and CCSD(T)-F12b/aug-cc-pV*n*Z [*n* = 2, 3 and 4] levels of theory are summarized in Tables 1 and 2. Taking a cue from previous studies on the $HOO^-/ClO^- + CH_3Cl$ and $HO^- + CH_3F$ reactions,[40,65,69,95] in addition to the typical S_N2 ($CH_3OOH + Y^-$) and proton-abstraction ($CH_2Y^- + H_2O_2$) routes, alternative channels of peroxide ion substitution (CH_3OO^- + HY), S_N2-induced elimination (CH_2O + HY + HO^-) and S_N2-induced rearrangement ($CH_2(OH)O^-$ + HY) are also analyzed. It should be noted that in the case of the $HOO^- + CH_3Cl$ reaction, the dynamical characterization reported by Xie and co-workers did not reveal the existence of the corresponding peroxide ion substitution, S_N2-induced rearrangement and proton abstraction, presumably, due to the fact that overall 1154 trajectories were run at one sole collision energy of 0.9 kcal mol^{-1}.[95] However, the pathways of peroxide ion substitution and S_N2-induced rearrangement were also considered in the course of their stationary-point survey.

As seen in Fig. 1, in the entrance channel of the back-side attack Walden inversion, several H-bonded stationary points can be found for $HOO^- + CH_3Y$: HMIN1 [Y = F, Cl, Br and I], HTS1 [Y = F, Cl, Br and I], HMIN2 [Y = Br and I] and HTS2 [Y = Cl, Br and I]. The energetics of these minima and transition states are similar, and the differences in the relative energies are within ∼1.5 kcal mol^{-1}. Moreover, the typical PreMIN ion–dipole complex does not demonstrate notable distinctions, as well. On the other hand, for the alternative pre-reaction halogen-bonded complex pathway, a different situation can be found. In line with $HO^- + CH_3Y$,[24,38] FSMIN is situated above HMIN1 by 13.2 (12.8) and 6.0 (5.6) kcal mol^{-1} for Y = Cl and Br, in order; while for Y = I, FSMIN is below HMIN1 by 4.5 (4.7) kcal mol^{-1}. Note that the back-side attack Walden-inversion mechanism is submerged except for Y = F, where HBTS is positioned above the reactant asymptote by 1.1 (1.4) kcal mol^{-1}. With the atomic number of Y, the barrier height of HBTS is increasing: 3.9 (3.7), 10.1 (10.2) and 18.7 (18.7) kcal mol^{-1} relative to the corresponding FSMIN, for Y = F, Cl, Br and I, respectively. The deep well of the FSMIN complex at Y = I points out the common occurrence of the front-side complex formation mechanism in S_N2 reactions involving CH_3I.[48,60,109] The energy profile of the conventional stationary points of the Walden-inversion pathway (PreMIN → WaldenTS → WaldenPostMIN/PostHMIN) is also profoundly comparable with that of the HO^- case.[24,38] For instance, the classical (adiabatic) barrier heights of WaldenTS are 10.3 (10.1), 2.3 (2.2) and 0.2 (0.1) kcal mol^{-1} for Y = F, Cl and Br, respectively, while in the case of HO^- at the same level of theory, these values are 11.2 (11.4), 2.4 (2.4) and 0.2 (0.1) kcal mol^{-1}, in the same order. The global minimum of S_N2 is also located at PostHMIN, although, compared to $HO^- + CH_3Y$, higher classical energies of −49.7, −65.6, −70.9 and −74.7 kcal mol^{-1} can be determined for HOO^- in the case of Y = F, Cl, Br and I, respectively. In tandem with this, a notable disparity emerges in the reaction enthalpies of the S_N2 channels: $HOO^- + CH_3Y$ happens to be more endothermic by exactly 6.1 kcal mol^{-1} in all cases. As a result, in the case of the S_N2 reactions of HOO^-, larger dissociation energies can be observed for the leaving Y^- at PostHMIN, indicating a more significant post-reaction hydrogen-bonded complex formation. Here, one may highlight the relevance of peroxide ion substitution, as well, because the formation of the CH_3OO^- + HY products is also more exothermic than that of the HO^- cases, predicting a substantially increased probability for peroxide ion substitution, especially for $HOO^- + CH_3F$.[40] WaldenPostHMIN also plays a significant role, as Zhao *et al.*[95] uncovered, and the reaction can proceed through this minimum towards PostTS, leading to the unusual CH_2O + HY + HO^- products. In the case of Y = Cl, WaldenPostHMIN could not be identified at the CCSD(T)-F12b/aug-cc-pV*n*Z [*n* = 2, 3] levels of theory. It is noteworthy that for Y = F, the novel mechanism of S_N2-induced elimination is exceedingly more exothermic than S_N2, submerged by 29.9 (36.3) kcal mol^{-1}. The global minimum of the PES is situated at the double H-bonded PostDHMIN complex, and the most exothermic process corresponds to the S_N2-induced rearrangement channel, but it is supposedly an improbable reaction route considering the multiple bond-breaking and -forming processes involved. Concerning the S_N2 pathways that result in the retention of the initial CH_3Y configuration, two different transition states (FSTS1 and FSTS2) can be identified for front-side attacks. According to the study of Ma *et al.*,[110] double inversion may not be an IRC path through a DITS-like transition state; despite that, theoretical investigations underscored its crucial character in the mechanism.[111,112] Similarly to the HO^- case, the transition state of double inversion has lower energy than that of front-side attack; however, no submerged DITS can be obtained.[24,38] The most endothermic channel is proton abstraction with reaction enthalpies

Table 2 The best available experimental and our benchmark *ab initio* 0 K reaction enthalpies (kcal mol^{-1}) of several product channels for the HOO^- + CH_3Y [Y = F, Cl, Br, I] reactions

	MP2	CCSD(T)-F12b					
HOO^- + CH_3F	DZ[a]	DZ[b]	TZ[c]	QZ[d]	ΔZPE[e]	Adiabatic[f]	Experiment[g]
CH_3OOH + F^-	−18.24	−13.38	−13.06	−13.13	1.46	−11.67	−11.82 ± 0.14
CH_2F^- + H_2O_2	34.54	34.87	35.22	35.32	−1.84	33.48	—
CH_3OO^- + HF	−11.24	−10.28	−10.08	−10.02	−1.11	−11.12	−11.00 ± 0.15
CH_2O + HF + HO^-	−51.98	−43.50	−42.94	−43.06	−4.92	−47.98	−47.99 ± 0.10
$CH_2(OH)O^-$ + HF	−85.40	−79.85	−79.22	−79.15	−0.70	−79.85	—
HOO^- + CH_3Cl	MP2[a]	DZ[b]	TZ[c]	QZ[d]	ΔZPE[e]	Adiabatic[f]	Experiment[g]
CH_3OOH + Cl^-	−48.79	−45.72	−45.61	−45.83	2.44	−43.39	−43.07 ± 0.14
CH_2Cl^- + H_2O_2	22.01	21.82	21.80	21.81	−1.33	20.48	21.64 ± 0.49
CH_3OO^- + HCl	−3.64	−3.44	−3.10	−2.89	−1.77	−4.66	−4.31 ± 0.14
CH_2O + HCl + HO^-	−44.38	−36.66	−35.97	−35.93	−5.58	−41.51	−41.30 ± 0.09
$CH_2(OH)O^-$ + HCl	−77.81	−73.01	−72.24	−72.02	−1.36	−73.39	—
HOO^- + CH_3Br	MP2[a]	DZ[b]	TZ[c]	QZ[d]	ΔZPE[e]	Adiabatic[f]	Experiment[g]
CH_3OOH + Br^-	−54.91	−54.21	−53.65	−53.98	2.85	−51.14	−50.60 ± 0.14
CH_2Br^- + H_2O_2	18.32	16.94	17.14	17.15	−1.17	15.98	—
CH_3OO^- + HBr	−0.72	−1.04	−0.51	−0.37	−1.86	−2.23	−1.85 ± 0.14
CH_2O + HBr + HO^-	−41.46	−34.26	−33.37	−33.41	−5.68	−39.08	−38.84 ± 0.10
$CH_2(OH)O^-$ + HBr	−74.89	−70.61	−69.65	−69.50	−1.46	−70.96	—
HOO^- + CH_3I	MP2[a]	DZ[b]	TZ[c]	QZ[d]	ΔZPE[e]	Adiabatic[f]	Experiment[g]
CH_3OOH + I^-	−61.29	−60.78	−60.32	−60.89	3.25	−57.64	−56.97 ± 0.14
CH_2I^- + H_2O_2	13.49	11.84	11.92	11.84	−0.95	10.89	—
CH_3OO^- + HI	2.44	1.68	2.14	2.24	−1.93	0.32	0.83 ± 0.14
CH_2O + HI + HO^-	−38.30	−31.54	−30.72	−30.80	−5.74	−36.54	−36.16 ± 0.10
$CH_2(OH)O^-$ + HI	−71.72	−67.89	−67.00	−66.89	−1.52	−68.41	—

[a] MP2/aug-cc-pVDZ. [b] CCSD(T)-F12b/aug-cc-pVDZ. [c] CCSD(T)-F12b/aug-cc-pVTZ. [d] CCSD(T)-F12b/aug-cc-pVQZ at CCSD(T)-F12b/aug-cc-pVTZ geometry. [e] ΔZPE(CCSD(T)-F12b/aug-cc-pVTZ). [f] QZ + ΔZPE. [g] Data obtained from the latest version (1.130) of the Active Thermochemical Tables (ATcT).[113,114] The uncertainties are derived using the Gaussian error-propagation law on the uncertainties of each 0 K enthalpy of formation provided in ATcT.

of 33.5 (F), 20.5 (Cl), 16.0 (Br) and 10.9 (I) kcal mol^{-1}. The entrance channel of proton abstraction is found to be the same as that for S_N2 and is supported by IRC calculations, in which three stationary points (two minima and one transition state) are explored along the pathway: ABSTS [Y = F, Cl, Br and I], ABSMIN1 [Y = Br and I], and ABSMIN2 [Y = F, Cl, Br and I].

The structures of the stationary points featuring the selected bond lengths and angles are shown in Fig. 2. The associated stationary points in the reactant channels (HMIN1/HTS1 and HMIN2/HTS2) demonstrate slight differences in their geometries, and the most pronounced disparity is discerned in the orientation of the corresponding HOO^- group. Regarding WaldenTS, two distinct structures are characterized depending on Y: the dihedral angle of O–O···C–H is ∼180° (*trans* arrangement) at Y = F, whereas a value of ∼0° (*cis* arrangement) is obtained at Y = Cl and Br, as seen in Fig. 2. According to earlier investigations on S_N2 reactions, similar discrepancies observed at CH_3F are not uncommon;[24] for instance, in the case of HO^- + CH_3Y,[38] for Y = Cl, Br and I FSTS has C_s symmetry, while for Y = F, the symmetry is broken. It should be noted that previous studies on the HOO^- + CH_3Cl S_N2 reaction reported a *trans* alignment for the O–O···C–H torsion angle of WaldenTS computed at the MP2/6-311++G(d,p) level of theory.[96,97] The geometries of PreMIN and WaldenTS defined in the early work of Evanseck *et al.* are discrepant from our benchmark results due to their implemented symmetry-constrained geometry optimizations.[74] Moreover, Ren *et al.* revealed two different transition states for Walden inversion with a *trans* alignment of the corresponding O–O···C–H torsion angle for both cases.[78] Nevertheless, in other investigations, the geometry of the uncovered WaldenTS of HOO^- + CH_3Cl is in accordance with that presented in this benchmark work.[79,88,95] It should also be highlighted that Wu *et al.* identified PreMIN and WaldenTS for Y = I at the MP2/6-311++G(d,p) level of theory,[96] although, in the course of the present study, WaldenTS cannot be found for Y = I at the MP2/aug-cc-pVDZ and CCSD(T)-F12b/aug-cc-pV*n*Z [*n* = 2, 3] levels of theory. Hence, the issues regarding these stationary points underline the relevance of employing higher-level *ab initio* methods for theoretical investigations. Concerning PostHMIN, alternative conformational isomers cannot be determined in contrast to the HO^- + CH_3F reaction.[40] As shown in Fig. 2, the transition states of the front-side attack mechanism differ from each other in the orientation of the HOO^- group, and owing to the additional Y···HO bond, FSTS2 is below FSTS1 in the case of Y = F and Cl. It is noteworthy that all the stationary-point characterizations can be performed without imposing symmetry restrictions, except for ABSMIN1, which has C_s symmetry. There are cases, where a C_s symmetry

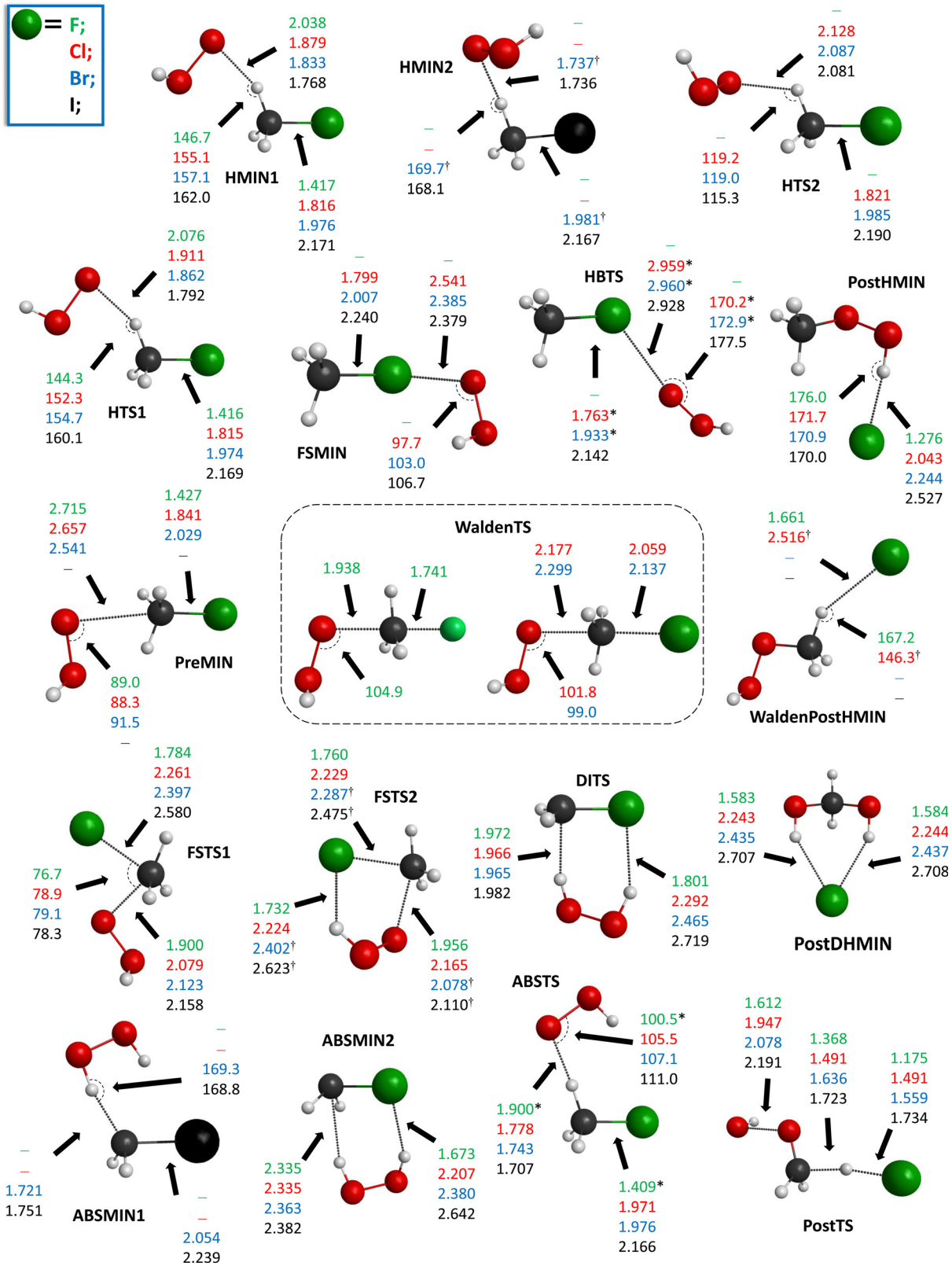

Fig. 2 Structures of the stationary points of the HOO^- + CH_3Y [Y = F, Cl, Br, I] reactions showing the most important bond lengths (Å) and angles (°) obtained at the CCSD(T)-F12b/aug-cc-pVTZ level of theory. † MP2/aug-cc-pVDZ structure; *CCSD(T)-F12b/aug-cc-pVDZ structure. Note that for Y = F at WaldenTS, a distinct structure can be identified compared to the case of Y = Cl and Br.

would also be expected (*e.g.*, HTS1, ABSTS); however, the corresponding geometry optimizations do not converge. The most accurate, CCSD(T)-F12b/aug-cc-pVTZ Cartesian coordinates of the stationary points, as well as of reactants and products, are provided in the ESI.†

The calculated classical and adiabatic *ab initio* relative energies of the products and the available "experimental" reaction enthalpies obtained from the active thermochemical tables (ATcT)[113,114] are given in Table 2. The benchmark structures of the reactants and products are shown in Fig. 3. The reaction enthalpies of S_N2 and proton abstraction decrease with increasing atomic weight of Y, whereas for the other pathways, a reverse tendency is revealed. Alongside the proton-abstraction channels for Y = F, Cl, Br and I, peroxide ion substitution is also an endothermic pathway in the case of Y = I. It is notable that for Y = F, the difference between the reaction enthalpies of S_N2 and peroxide ion substitution is only 0.5 kcal mol^{-1}. In most instances, our benchmark results are in satisfactory agreement with the experimental data, except for the CH_2Cl^- + H_2O_2 products, where a difference of 1.2 kcal mol^{-1} emerges. However, it should be noted that the derived uncertainty of the experimental reaction enthalpy is remarkably substantial (±0.5 kcal mol^{-1}). Similarly, for the F^- + CH_3Cl → CH_2Cl^- + HF proton-abstraction channel, a large deviation (0.9 kcal mol^{-1}) can also be observed between the experimental and our calculated benchmark reaction enthalpy with a significant uncertainty (0.5 kcal mol^{-1}) of the experimental value.[112] Thus, these cases may highlight the inaccuracy of the available 0 K enthalpy of formation for CH_2Cl^- in the ATcT. In the case of the HOO^- + CH_3Y [Y = F and Cl] S_N2 reactions, the reaction energies of −13.0 (F) and −45.3 (Cl) kcal mol^{-1}, obtained by Wu *et al.* utilizing CCSD(T)/aug-cc-pVTZ(-PP) energy calculations at the MP2/6-311++G(d,p) geometries,[96], in kcal mol^{-1} are in conformity with our benchmark values of −13.0 (F) and −45.8 (Cl) kcal mol^{-1}. Although, for Y = Br and I, their S_N2 reaction energies of −50.9 and −56.4 kcal mol^{-1} are higher than our results by 3.1 and 4.5 kcal mol^{-1}, respectively. The classical energies of the stationary points of the present work can also be compared with the results of Wu *et al.*[96] They characterized five stationary points (HMIN1, HTS2, PreMIN, WaldenTS and PostHMIN) along the back-side attack Walden inversion, mainly, their computed CCSD(T)/aug-cc-pVTZ(-PP) energies are in good agreement with our benchmark data. In an earlier study on HOO^- + CH_3Cl by Zhao *et al.*,[95] the reported energies of PreMIN and PostHMIN at the MP2/6-31+G(d,p) level of theory are in good agreement with the present benchmark values. For WaldenTS, a difference of more than 2 kcal mol^{-1} occurs; moreover, an enormous deviation of 13.2 kcal mol^{-1} is obtained at Walden-PostHMIN, remarkably. Motivated by this discrepancy, we characterized the corresponding stationary points of HOO^- + CH_3Cl at the MP2/6-31+G(d,p) level of theory using the Molpro program package.[108] In the course of computations, spherical harmonic basis functions are used; however, it is noteworthy that by employing Cartesian functions, comparable relative energies can be obtained within ±0.3 kcal mol^{-1}. Our obtained MP2/6-31+G(d,p) classical energies of −14.9 (PreMIN), −10.5 (WaldenTS), −64.6 (PostHMIN), −53.2 (WaldenPostHMIN), −31.5 (PostTS), and −136.5 (PostDHMIN), in kcal mol^{-1}, are in conformity with the benchmark data. While our optimized structures of the stationary points show satisfactory alignment with those determined by Zhao *et al.*,[95] significant inexplicable disparities are unveiled for the classical energies in a few cases. We also determined the classical (adiabatic) energies of the products at the MP2/6-31+G(d,p) level; CH_2Cl^- + H_2O_2: 29.4 (27.7), CH_3OOH + Cl^- −45.7 (−43.5), CH_3OO^- + HCl: −2.1 (−3.7), CH_2O + HCl + HO^-: −40.0 (−45.8) and $CH_2(OH)O^-$ + HCl: −75.2 (−76.8), in kcal mol^{-1}. It can be seen that for certain cases, the provided energies differ from the experiment by more than 4 kcal mol^{-1}; especially for proton abstraction, an enormous difference of 6.1 kcal mol^{-1} occurs, which casts doubt on the reliability of MP2/6-31+G(d,p). The G2+ adiabatic energies of WaldenTS (−13.5 kcal mol^{-1}) and the S_N2 products (−43.2 kcal mol^{-1}), computed by Ren *et al.* for HOO^- + CH_3Cl, are also in consonance with the present study.[79]

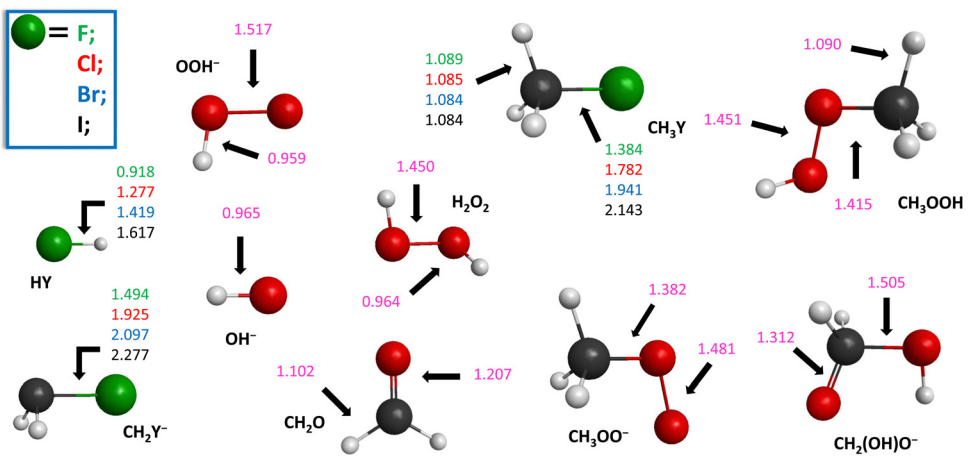

Fig. 3 Structures of the reactants and products of the HOO^- + CH_3Y [Y = F, Cl, Br, I] reactions showing the most important bond lengths (Å) obtained at the CCSD(T)-F12b/aug-cc-pVTZ level of theory.

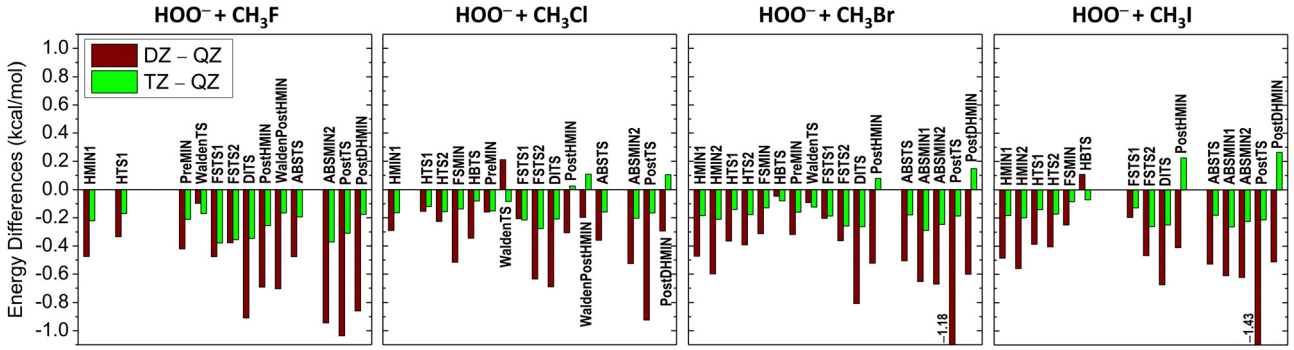

Fig. 4 Convergence of the CCSD(T)-F12b relative energies for the stationary points of the HOO^- + CH_3Y [Y = F, Cl, Br, I] reactions utilizing the aug-cc-pVDZ (DZ), aug-cc-pVTZ (TZ) and aug-cc-pVQZ (QZ) basis sets.

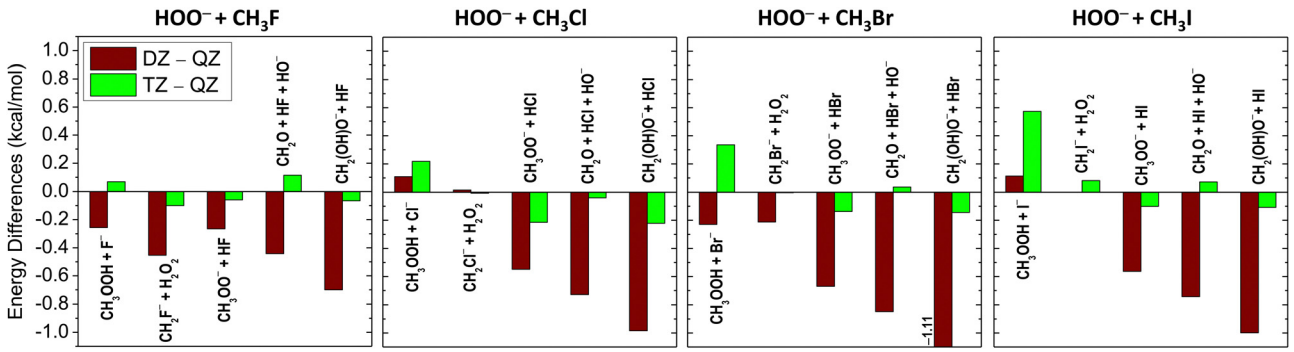

Fig. 5 Convergence of the CCSD(T)-F12b relative energies for the product channels of the HOO^- + CH_3Y [Y = F, Cl, Br, I] reactions utilizing the aug-cc-pVDZ (DZ), aug-cc-pVTZ (TZ) and aug-cc-pVQZ (QZ) basis sets.

As shown in Fig. 4 and 5, the basis-set convergence of the CCSD(T)-F12b relative energies is also investigated for the title reactions. In most cases, a fast and smooth basis-set convergence can be recognized, except for WaldenTS [Y = F and Br], HBTS [Y = Br], FSTS1 [Y = Cl] and $CH_3OOH + Y^-$ [Y = Cl, Br and I], as in these instances the relative energy differences between aug-cc-pVDZ (DZ) and aug-cc-pVQZ (QZ) are smaller than the corresponding values of aug-cc-pVTZ (TZ) and QZ. The largest differences emerge at PostTS [Y = Br and I] and $CH_2(OH)O^-$ + HBr, where the deviations between the DZ and QZ relative energies are found to be in the range of 1.1–1.4 kcal mol^{-1}. In contrast, the energy differences between TZ and QZ are within ±0.4 kcal mol^{-1}, except at $CH_3OOH + I^-$ (0.57 kcal mol^{-1}). Regarding the ZPE effects, the most significant contributions appear at the post-reaction stationary points (PostHMIN, WaldenPostHMIN, PostTS and PostDHMIN) and for the products of $CH_3OOH + Y^-$ and CH_2O + HY + HO^-. The vast majority of the stationary points have positive ZPE corrections, whereas, in the case of the reaction channels, positive ZPE effects occur only for the $CH_3OOH + Y^-$ products.

IV. Summary and conclusions

In this study, we have characterized the complex potential energy surfaces of the HOO^- + CH_3Y [Y = F, Cl, Br and I] reactions using the modern explicitly-correlated CCSD(T)-F12b method with the aug-cc-pV*n*Z [*n* = 2–4] basis sets. For S_N2, we have considered the pathways of back-side attack Walden inversion, front-side attack, double inversion[19] and halogen-bonded complex formation.[48] In most cases, the entrance channel of HOO^- + CH_3Y comprises seven stationary points: two H-bonded, a front-side halogen-bonded and a traditional ion–dipole minima, as well as two H-bonded and front-side halogen-bonded transition states. Similar to the HO^- + CH_3Y S_N2 reactions,[24,38] no typical transition state has been identified for the Walden inversion in the case of Y = I, and in light of the discrepancy of the earlier findings, we have clarified the accurate structure of the Walden-inversion transition state for Y = Cl. In the exit channel of S_N2, two H-bonded minima are situated: $Y^-\cdots HOOCH_3$ and $Y^-\cdots HCH_2OOH$. Based on the findings of Xie and co-workers,[95] the HOO^- + CH_3Cl reaction can proceed through $Cl^-\cdots HCH_2OOH$ towards the $[Cl\cdots H\cdots CH_2O\cdots OH]^-$ transition state generating the unusual products of CH_2O + HCl + HO^-. It should be highlighted that for HOO^- + CH_3F, the reaction enthalpy of this novel S_N2-induced elimination is more negative by 36.3 kcal mol^{-1} than the corresponding S_N2 process. Concerning the retention paths of S_N2, two distinct transition states have been recognized for front-side attacks, and as observed for HO^- + CH_3Y, double inversion is a lower-energy process than front-side attack.[24,38] Building upon the earlier work of Xie and co-workers,[95] besides S_N2-induced elimination, we have also investigated other channels such as proton abstraction (CH_2Y^- + H_2O_2), peroxide ion substitution (CH_3OO^- + HY) and

S_N2-induced rearrangement ($CH_2(OH)O^-$ + HY). In the case of Y = F, Cl and Br, the peroxide ion substitution has been found to be exothermic with reaction enthalpies of −11.1 (F), −4.7 (Cl) and −2.2 (Br) kcal mol^{-1}. The most exothermic path is S_N2-induced rearrangement; however, it is presumed to be an improbable reaction channel due to the complex bond-breaking and -forming processes involved. The benchmark reaction enthalpies presented in this work are usually in excellent agreement with those obtained from ATcT.[113,114] We have also assessed the basis-set convergence of the CCSD(T)-F12b method and the ZPE contributions of the stationary points.

We are confident that the present benchmark characterization of HOO^- + CH_3Y supports further theoretical and experimental investigations regarding reaction dynamics as well as the influence of the α-effect related to HOO^-.

Conflicts of interest

There are no conflicts of interest to declare.

Acknowledgements

We acknowledge the financial support of the National Research, Development and Innovation Office-NKFIH, K-125317 and K-146759; project no. TKP2021-NVA-19 provided by the Ministry of Innovation and Technology of Hungary from the National Research, Development and Innovation Fund, financed under the TKP2021-NVA funding scheme; the National Young Talent Scholarship (Grant no. NTP-NFTÖ-22-B-0050 for D. A. T.); and the Momentum (Lendület) Program of the Hungarian Academy of Sciences.

References

1 A. Dedieu and A. Veillard, *J. Am. Chem. Soc.*, 1972, **94**, 6730.
2 W. N. Olmstead and J. I. Brauman, *J. Am. Chem. Soc.*, 1977, **99**, 4219.
3 A. Merkel, R. Zahradník and Z. Havlas, *J. Am. Chem. Soc.*, 1988, **110**, 8355.
4 S. S. Shaik, H. B. Schlegel and S. Wolfe, *Theoretical Aspects of Physical Organic Chemistry: The S_N2 Mechanism,* Wiley, New York, 1992.
5 W. L. Hase, *Science*, 1994, **266**, 998.
6 M. L. Chabinyc, S. L. Craig, C. K. Regan and J. I. Brauman, *Science*, 1998, **279**, 1882.
7 J. K. Laerdahl and E. Uggerud, *Int. J. Mass Spectrom.*, 2002, **214**, 277.
8 E. Uggerud, *Adv. Phys. Org. Chem.*, 2017, **51**, 1.
9 T. A. Hamlin, M. Swart and F. M. Bickelhaupt, *ChemPhysChem*, 2018, **19**, 1315.
10 R. Wester, *Mass Spectrom. Rev.*, 2022, **41**, 627.
11 A. J. R. Heck and D. W. Chandler, *Annu. Rev. Phys. Chem.*, 1995, **46**, 335.
12 M. N. R. Ashfold, N. H. Nahler, A. J. Orr-Ewing, O. P. J. Vieuxmaire, R. L. Toomes, T. N. Kitsopoulos, I. A. Garcia, D. A. Chestakov, S. M. Wu and D. H. Parker, *Phys. Chem. Chem. Phys.*, 2006, **8**, 26.
13 D. C. Clary, *Proc. Natl. Acad. Sci. U. S. A.*, 2008, **105**, 12649.
14 J. Mikosch, S. Trippel, C. Eichhorn, R. Otto, U. Lourderaj, J. X. Zhang, W. L. Hase, M. Weidemüller and R. Wester, *Science*, 2008, **319**, 183.
15 J. Meyer and R. Wester, *Annu. Rev. Phys. Chem.*, 2017, **68**, 333.
16 J. Li, B. Zhao, D. Xie and H. Guo, *J. Phys. Chem. Lett.*, 2020, **11**, 8844.
17 J. I. Brauman, *Science*, 2008, **319**, 168.
18 P. Manikandan, J. Zhang and W. L. Hase, *J. Phys. Chem. A*, 2012, **116**, 3061.
19 I. Szabó and G. Czakó, *Nat. Commun.*, 2015, **6**, 5972.
20 M. Stei, E. Carrascosa, M. A. Kainz, A. H. Kelkar, J. Meyer, I. Szabó, G. Czakó and R. Wester, *Nat. Chem.*, 2016, **8**, 151.
21 J. Xie and W. L. Hase, *Science*, 2016, **352**, 32.
22 L. Sun, K. Song and W. L. Hase, *Science*, 2002, **296**, 875.
23 L. Sun, K. Song, W. L. Hase, M. Sena and J. M. Riveros, *Int. J. Mass Spectrom.*, 2003, **227**, 315.
24 D. A. Tasi, Z. Fábián and G. Czakó, *Phys. Chem. Chem. Phys.*, 2019, **21**, 7924.
25 S. R. Hare, L. A. Bratholm, D. R. Glowacki and B. K. Carpenter, *Chem. Sci.*, 2019, **10**, 9954.
26 T. Tsutsumi, Y. Ono, Z. Arai and T. Taketsugu, *J. Chem. Theory Comput.*, 2020, **16**, 4029.
27 D. A. Tasi, C. Tokaji and G. Czakó, *Phys. Chem. Chem. Phys.*, 2021, **23**, 13526.
28 T. Tsutsumi, Y. Ono and T. Taketsugu, *Chem. Commun.*, 2021, **57**, 11734.
29 T. Tsutsumi, Y. Ono and T. Taketsugu, *Top. Curr. Chem.*, 2022, **380**, 19.
30 S. Zhao, G. Fu, W. Zhen, L. Yang, J. Sun and J. Zhang, *Phys. Chem. Chem. Phys.*, 2022, **24**, 24146.
31 H. Tachikawa, M. Igarashi and T. Ishibashi, *J. Phys. Chem. A*, 2002, **106**, 10977.
32 H. Tachikawa and M. Igarashi, *Chem. Phys.*, 2006, **324**, 639.
33 H. Yin, D. Wang and M. Valiev, *J. Phys. Chem. A*, 2011, **115**, 12047.
34 Y. Xu, T. Wang and D. Wang, *J. Chem. Phys.*, 2012, **137**, 184501.
35 S. Giri, E. Echegaray, P. W. Ayers, A. S. Nuñez, F. Lund and A. Toro-Labbé, *J. Phys. Chem. A*, 2012, **116**, 10015.
36 J. Chen, Y. Xu and D. Wang, *J. Comput. Chem.*, 2014, **35**, 445.
37 T. Tsutsumi, Y. Ono, Z. Arai and T. Taketsugu, *J. Chem. Theory Comput.*, 2018, **14**, 4263.
38 D. A. Tasi, Z. Fábián and G. Czakó, *J. Phys. Chem. A*, 2018, **122**, 5773.
39 Y. G. Proenza, M. A. F. de Souza and R. L. Longo, *Chem. – Eur. J.*, 2016, **22**, 16220.
40 D. A. Tasi and G. Czakó, *Chem. Sci.*, 2021, **12**, 14369.
41 J. Qin, Y. Liu and J. Li, *J. Chem. Phys.*, 2022, **157**, 124301.
42 R. Otto, J. Brox, S. Trippel, M. Stei, T. Best and R. Wester, *Nat. Chem.*, 2012, **4**, 534.
43 J. Xie, R. Otto, J. Mikosch, J. Zhang, R. Wester and W. L. Hase, *Acc. Chem. Res.*, 2014, **47**, 2960.

44 J. Xie, J. Zhang and W. L. Hase, *Int. J. Mass Spectrom.*, 2015, **378**, 14.
45 J. Xie, R. Otto, R. Wester and W. L. Hase, *J. Chem. Phys.*, 2015, **142**, 244308.
46 E. Carrascosa, J. Meyer and R. Wester, *Chem. Soc. Rev.*, 2017, **46**, 7498.
47 J. Xie, X. Ma, J. Zhang, P. M. Hierl, A. A. Viggiano and W. L. Hase, *Int. J. Mass Spectrom.*, 2017, **418**, 122.
48 X. Ji, C. Zhao and J. Xie, *Phys. Chem. Chem. Phys.*, 2021, **23**, 6349.
49 R. Otto, J. Xie, J. Brox, S. Trippel, M. Stei, T. Best, M. R. Siebert, W. L. Hase and R. Wester, *Faraday Discuss.*, 2012, **157**, 41.
50 J. Xie, R. Sun, M. R. Siebert, R. Otto, R. Wester and W. L. Hase, *J. Phys. Chem. A*, 2013, **117**, 7162.
51 J. Xie, S. C. Kohale, W. L. Hase, S. G. Ard, J. J. Melko, N. S. Shuman and A. A. Viggiano, *J. Phys. Chem. A*, 2013, **117**, 14019.
52 J. Xie, J. Zhang, R. Sun, R. Wester and W. L. Hase, *Int. J. Mass Spectrom.*, 2019, **438**, 115.
53 D. A. Tasi, T. Győri and G. Czakó, *Phys. Chem. Chem. Phys.*, 2020, **22**, 3775.
54 T. Győri and G. Czakó, *J. Chem. Theory Comput.*, 2020, **16**, 51.
55 D. A. Tasi, T. Michaelsen, R. Wester and G. Czakó, *Phys. Chem. Chem. Phys.*, 2023, **25**, 4005.
56 S. Rao and D. Wang, *Chin. J. Chem. Phys.*, 2023, **36**, 169.
57 D. A. Tasi and G. Czakó, *J. Chem. Phys.*, 2024, **160**, 044305.
58 E. Carrascosa, M. Bawart, M. Stei, F. Linden, F. Carelli, J. Meyer, W. D. Geppert, F. A. Gianturco and R. Wester, *J. Chem. Phys.*, 2015, **143**, 184309.
59 Z. Kerekes, D. A. Tasi and G. Czakó, *J. Phys. Chem. A*, 2022, **126**, 889.
60 D. A. Tasi and G. Czakó, *J. Chem. Phys.*, 2022, **156**, 184306.
61 X. Liu, S. Tian, B. Pang, H. Li and Y. Wu, *Phys. Chem. Chem. Phys.*, 2023, **25**, 14812.
62 X. Liu, W. Guo, H. Feng, B. Pang and Y. Wu, *J. Phys. Chem. A*, 2023, **127**, 7373.
63 A. Gutal and M. Paranjothy, *Phys. Chem. Chem. Phys.*, 2023, **25**, 15015.
64 W. P. Hu and D. G. Truhlar, *J. Am. Chem. Soc.*, 1996, **118**, 860.
65 S. M. Villano, N. Eyet, W. C. Lineberger and V. M. Bierbaum, *J. Am. Chem. Soc.*, 2009, **131**, 8227.
66 L. Junxi, W. Yanbin, Z. Qiang, L. Yu, G. Zhiyuan and W. Xiuhong, *J. Mol. Model.*, 2013, **19**, 1739.
67 L. Junxi, S. Qiong, L. Yu, Z. Qiang and G. Zhiyuan, *Can. J. Chem.*, 2014, **92**, 868.
68 L. Junxi, S. Qiong, W. Yanbin and G. Zhiyuan, *Bull. Chem. Soc. Jpn.*, 2015, **88**, 110.
69 F. Yu, *J. Phys. Chem. A*, 2016, **120**, 1813.
70 L. Yun-Yun, Q. Fang-Zhou, Z. Jun, R. Yi and L. Kai-Chung, *J. Mol. Model.*, 2017, **23**, 192.
71 T. Hansen, P. Vermeeren, F. M. Bickelhaupt and T. A. Hamlin, *Angew. Chem., Int. Ed.*, 2021, **60**, 20840.
72 S. Hoz and E. Buncel, *Isr. J. Chem.*, 1985, **26**, 313.
73 J. O. Edwards and R. G. Pearson, *J. Am. Chem. Soc.*, 1962, **84**, 16.
74 J. D. Evanseck, J. F. Blake and W. L. Jorgensen, *J. Am. Chem. Soc.*, 1987, **109**, 2349.
75 E. Buncel and I. H. Um, *Tetrahedron*, 2004, **60**, 7801.
76 C. H. DePuy, E. W. Della, J. Filley, J. J. Grabowski and V. M. Bierbaum, *J. Am. Chem. Soc.*, 1983, **105**, 2481.
77 E. V. Patterson and K. R. Fountain, *J. Org. Chem.*, 2006, **71**, 8121.
78 Y. Ren and H. Yamataka, *Org. Lett.*, 2006, **8**, 119.
79 Y. Ren and H. Yamataka, *Chem. – Eur. J.*, 2007, **13**, 677.
80 Y. Ren and H. Yamataka, *J. Org. Chem.*, 2007, **72**, 5660.
81 A. M. McAnoy, M. R. L. Paine and S. J. Blanksby, *Org. Biomol. Chem.*, 2008, **6**, 2316.
82 Y. I. Ren and H. Yamataka, *J. Comput. Chem.*, 2009, **30**, 358.
83 J. M. Garver, S. Gronert and V. M. Bierbaum, *J. Am. Chem. Soc.*, 2011, **133**, 13894.
84 J. M. Garver, Z. Yang, N. Wehres, C. M. Nichols, B. B. Worker and V. M. Bierbaum, *Int. J. Mass Spectrom.*, 2012, **330–332**, 182.
85 Y. Ren, X. G. Wei, S. J. Ren, K. C. Lau, N. B. Wong and W. K. Li, *J. Comput. Chem.*, 2013, **34**, 1997.
86 I. H. Um, L. R. Im and E. Buncel, *J. Org. Chem.*, 2010, **75**, 8571.
87 X. G. Wei, X. M. Sun, X. P. Wu, Y. Ren, N. B. Wong and W. K. Li, *J. Org. Chem.*, 2010, **75**, 4212.
88 D. L. Thomsen, J. N. Reece, C. M. Nichols, S. Hammerum and V. M. Bierbaum, *J. Am. Chem. Soc.*, 2013, **135**, 15508.
89 D. L. Thomsen, J. N. Reece, C. M. Nichols, S. Hammerum and V. M. Bierbaum, *J. Phys. Chem. A*, 2014, **118**, 8060.
90 D. L. Thomsen, C. M. Nichols, J. N. Reece, S. Hammerum and V. M. Bierbaum, *J. Am. Soc. Mass Spectrom.*, 2014, **25**, 159.
91 W. Y. Zhao, J. Yu, S. J. Ren, X. G. Wei, F. Z. Qiu, P. H. Li, H. Li, Y. P. Zhou, C. Z. Yin, A. P. Chen, H. Li, L. Zhang, J. Zhu, Y. Ren and K. C. Lau, *J. Comput. Chem.*, 2015, **36**, 844.
92 N. Singh, Y. Karpichev, R. Sharma, B. Gupta, A. K. Sahu, M. L. Satnami and K. K. Ghosh, *Org. Biomol. Chem.*, 2015, **13**, 2827.
93 E. Juaristi, G. Dos Passos Gomes, A. O. Terent'ev, R. Notario and I. V. Alabugin, *J. Am. Chem. Soc.*, 2017, **139**, 10799.
94 F. Yu, *J. Chem. Phys.*, 2018, **148**, 014302.
95 C. Zhao, X. Ma, X. Wu, D. L. Thomsen, V. M. Bierbaum and J. Xie, *J. Phys. Chem. Lett.*, 2021, **12**, 7134.
96 X. Wu, C. Zhao and J. Xie, *ChemPhysChem*, 2022, **23**, e202200285.
97 Y. Hu, X. Wu and J. Xie, *Phys. Chem. Chem. Phys.*, 2023, **25**, 1947.
98 D. J. Anick, *J. Phys. Chem. A*, 2011, **115**, 6327.
99 C. Møller and M. S. Plesset, *Phys. Rev.*, 1934, **46**, 618.
100 T. H. Dunning, *J. Chem. Phys.*, 1989, **90**, 1007.
101 R. Van de Vijver and J. Zádor, *Comput. Phys. Commun.*, 2020, **248**, 106947.
102 M. Kuwahara, Y. Harabuchi, S. Maeda, J. Fujima and K. Takahashi, *Digit. Discovery*, 2023, **2**, 1104.

103 E. Kraka, J. J. Antonio and M. Freindorf, *Chem. Commun.*, 2023, **59**, 7151.
104 K. Raghavachari, G. W. Trucks, J. A. Pople and M. Head-Gordon, *Chem. Phys. Lett.*, 1989, **157**, 479.
105 T. B. Adler, G. Knizia and H. J. Werner, *J. Chem. Phys.*, 2007, **127**, 221106.
106 G. Knizia, T. B. Adler and H. J. Werner, *J. Chem. Phys.*, 2009, **130**, 054104.
107 K. A. Peterson, D. Figgen, E. Goll, H. Stoll and M. Dolg, *J. Chem. Phys.*, 2003, **119**, 11113.
108 H.-J. Werner, P. J. Knowles, G. Knizia, F. R. Manby and M. Schütz, *et al.*, *Molpro, version 2015.1, a package of ab initio programs*, see **https://www.molpro.net**.
109 I. Szabó, B. Olasz and G. Czakó, *J. Phys. Chem. Lett.*, 2017, **8**, 2917.
110 Y.-T. Ma, X. Ma, A. Li, H. Guo, L. Yang, J. Zhang and W. L. Hase, *Phys. Chem. Chem. Phys.*, 2017, **19**, 20127.
111 B. Olasz and G. Czakó, *Phys. Chem. Chem. Phys.*, 2019, **21**, 1578.
112 G. Czakó, T. Győri, B. Olasz, D. Papp, I. Szabó, V. Tajti and D. A. Tasi, *Phys. Chem. Chem. Phys.*, 2020, **22**, 4298.
113 B. Ruscic, R. E. Pinzon, M. L. Morton, G. Von Laszevski, S. J. Bittner, S. G. Nijsure, K. A. Amin, M. Minkoff and A. F. Wagner, *J. Phys. Chem. A*, 2004, **108**, 9979.
114 D. H. Ruscic and B. Bross, *Active Thermochemical Tables (ATcT) values based on ver. 1.130 of the Thermochemical Network*, 2023, available at ATcT.anl.gov.